Improved Resistance to Laser Weld Heat-Affected Zone Microfissuring in a Newly Developed Superalloy HAYNES 282

L.O. OSOBA, R.G. DING, and O.A. OJO

Gleeble thermomechanical simulation and microstrucutural analyses of laser beam weldability of a newly developed precipitation-hardened nickel-base HAYNES alloy 282 were performed to better understand the fundamental cause of heat-affected zone (HAZ) cracking and how to prevent the cracking problem in the material. Submicron size intergranular M_5B_3 particles are identified for the first time in the present work by transmission electron microscopy, and were found to be the primary cause of HAZ grain boundary liquation cracking in the alloy. Complete dissolution of the liquating M_5B_3 particles by preweld heat treatment exacerbated rather than reduced susceptibility to cracking, which could be attributed to nonequilibrium intergranular segregation of boron atoms, liberated by the complete dissolution of the boride particles, during cooling from heat treatment temperature. Consequently, to reduce the HAZ cracking, a preweld heat treatment that reduces the volume fraction of the M_5B_3 particles while minimizing nonequilibrium grain boundary boron segregation is necessary, and this is possible by heat treating the alloy at 1353 K to 1373 K (1080 °C to 1100 °C). Further improvement in cracking resistance to produce crack-free welds is achieved by subjecting the alloy to thermomechanically induced grain refinement coupled with the preweld heat treatment at 1353 K (1080 °C). A Gleeble hot ductility test showed that formation of the crack-free welds is unexplainable by mere reduction in grain size without considering the effect of grain refinement on intergranular liquid produced by subsolidus liquation of the M_5B_3 borides.

DOI: 10.1007/s11661-012-1212-7

I. INTRODUCTION

COMPONENTS of aero and land-based gas turbine engines are manufactured from nickel-base superalloys because of their unique high strength at elevated temperatures and resistance to hot corrosion in severe hostile environments. In order to meet the ever increasing demand for better engine performance, it has become necessary for designers to increase turbine inlet temperatures. HAYNES 282* is a new γ' precipitation-strengthened nickel-base superalloy, developed to meet the challenges of higher turbine service temperatures. The alloy exhibits a unique combination of excellent creep properties and thermal stability that meet and surpass those of the commonly used superalloys, such as WASPALOY,** INCONEL 718,† HAYNES 263,‡ and RENE 41.§[1] Joining of simple or complex shape turbine parts is an essential aspect of the manufacturing process. Also, during service, hot section components of turbine engines are subjected to different forms of thermal and mechanical stresses for a prolonged period of time that inevitably cause damage and limit component useful service life. The increasing high cost of procuring new parts and

*HAYNES 282 is a trademark of Haynes International, Kokomo, IN.

**WASPALOY is a trademark of United Technologies Corp., Hartford, CT.

†INCONEL 718 is a trademark of Special Metals Corp., Huntington, WV.

‡HAYNES 263 is a trademark of Haynes International, Kokomo, IN.

§RENE is a trademark of General Electric Company, Fairfield, CT.

L.O. OSOBA, Doctoral Candidate, and O.A. OJO, Associate Professor, are with the Department of Mechanical and Manufacturing Engineering, University of Manitoba, Winnipeg, MB, Canada R3T 5V6. Contact e-mail: olanrewaju.ojo@ad.umanitoba.ca R.G. DING, Research Associate, is with the Department of Metallurgy and Materials Engineering, University of Birmingham, Birmingham B15 2TT, United Kingdom.

Manuscript submitted September 27, 2011.
Article published online September 1, 2012

associated delay in delivery time often necessitate that service-damaged components are repaired in preference to total replacement. Laser beam welding (LBW) has attracted considerable interest in recent years for the fabrication and repair of advanced high-temperature alloys due to its speed, flexibility, high-energy concentration, and power transfer rate to produce low heat input welds with reduced heat-affected zone (HAZ) and physical distortions. A recent study on LBW of HAYNES alloy 282 by the present authors has shown that the alloy is susceptible to cracking in the HAZ.[2] An adequate understanding of the factors responsible for the susceptibility of the alloy to HAZ cracking is crucial to developing an improved procedure for joining the alloy by LBW. Therefore, the objective of this research is to perform a detailed systematic study to better understand the primary cause of the HAZ cracking and develop a viable and effective approach for improving resistance of the newly developed superalloy to cracking during LBW. The results of this investigation are presented and discussed in this article.

II. MATERIAL AND EXPERIMENTAL PROCEDURES

Wrought HAYNES alloy 282 used in this study was provided by Haynes International Inc. in the form of mill bright-annealed plates of dimensions 610 × 120 × 11.5 mm. The nominal chemical composition of the material (wt pct) is 1.5Al, 2.1Ti, 10Co, 20Cr, 8.5Mo, 1.5Fe, 0.3Mn, 0.15Si, 0.06C, 0.005B, and balance nickel. Test specimens with dimensions 65 × 15 × 5 mm were machined from the as-received plate by numerically controlled wire electro-discharge machine (EDM). The machined specimens were subjected to the preweld heat treatments listed in Table I. The hardness values of the material in as-received and heat-treated conditions were measured by using the Vickers hardness testing machine. The preweld-heat-treated specimens were autogenously welded by a single-pass CO_2 laser beam by using the welding parameters listed in Table II. Welded specimens were sectioned transversely to the welding direction by the EDM to produce 10 sections from each weld specimen. Also, in order to evaluate the hot ductility of the alloy and to physically simulate the nonequilibrium microstructural changes in the HAZ during welding, a Gleeble 1500-D thermomechanical simulation system (Dynamic System Inc., Poestenkill, NY) was used. The simulation was performed at a rapid heating rate of 150 °C/s to peak temperatures that ranged from 1323 K to 1473 K (1050 °C to 1200 °C) and for different holding times, followed by water quenching to preserve, as much as possible, the microstructural changes that ensued at the peak temperatures. Selected specimens were pulled to failure in order to evaluate the hot ductility at various peak temperatures. As-received, preweld-heat-treated, welded, and Gleeble-simulated specimens were prepared by standard metallographic techniques for microstructural study. The metallographic specimens were chemically etched with the use of modified Kalling's reagent—40 mL distilled water + 480 mL HCl + 48 g of $CuCl_2$—and electrolytically etched in 10 pct Oxalic acid at 6 V for 3 to 5 seconds. The microstructures of the preweld-heat-treated, welded, and Gleeble-simulated specimens were initially examined by optical microscopy with the use of a Zeiss Axiovert 25 inverted-reflected light microscope (Carl Zeiss, Jena, Germany) equipped with Clemex Vision 3.0 image analysis software (Clemex Technologies Inc., Longueil, Canada). A more detailed microstructural study, spectroscopy analysis, and fractography examination were carried out by using a JEOL 5900 scanning electron microscope (SEM) and a FEI Tecnai F20 scanning transmission electron microscope (STEM). Both microscopes are equipped with an Oxford energy-dispersive spectrometer (EDS), and the Tecnai F20 is equipped with an X-Max Silicon Drift Detector. TEM specimens were prepared by mechanical grinding 3-mm-diameter discs to ~150 μm and then twin-jet electropolishing them in a solution of 10 pct perchloric acid, 30 pct butanol, and 60 pct methanol at 243 K (−30 °C) and 25 V. The extent of HAZ cracking was determined by measuring the total crack length in 10 sections of each welded specimen using the SEM (operated in both secondary and backscattered imaging modes). Major phase transformation temperatures in the alloy were determined using a Netzch 404C differential scanning calorimeter (DSC) (NETZSCH Instrument Inc., Burlington, MA). In addition, the characters of grain boundaries in the alloy were examined by carrying out electron backscatter diffraction (EBSD) based crystallographic orientation mapping by using a HKL Nordlys EBSD detector (developed by Oxford Instruments, Oxfordshire, UK), which was attached to a PHILIPS[§§] XL 30 SEM. Grain boundary segregation of boron was examined by a Cameca IMS-3f secondary ion mass spectrometer (SIMS) (CAMECA, Gennevilliers, France), using a primary ion beam of positive oxygen O_2^+. Mass resolved images of boron were obtained by imaging positive secondary ions of $^{11}B^+$, rastered over an approximately 150-μm-diameter surface.

[§§]PHILIPS is a trademark of FEI Company, Hillsboro, OR.

Table I. List of Preweld Heat Treatments

Heat Treatment
1323 K to 1423 K (1050 °C to 1150 °C)/2 h/WQ
1323 K to 1423 K (1050 °C to 1150 °C)/2 h/AC
1323 K to 1423 K (1050 °C to 1150 °C)/2 h/FC
1423 K (1150 °C)/2 h/WQ + 1283 K (1010 °C)/2 h AC + 1061 K (788 °C)/8 h AC
Material with refined grain size—1353 K (1080 °C)/2 hour/FC

AC—air-cooled, WQ—water-quenched, and FC—furnace-cooled.

Table II. Laser Beam Welding Parameters

Power (kW)	Speed (m min^{-1})	Beam Focus (mm)	Shielding Gas Flow Rate (L min^{-1})	Welding Gas Flow Rate (L min^{-1})
2	1.5	–2	30	25

III. RESULTS AND DISCUSSION

A. *Microstructure of HAYNES Alloy 282 in Standard-Heat-Treated Condition*

Figure 1 shows a SEM micrograph of the as-received alloy 282. The microstructure, with an average grain size ≈140 μm, consists of gamma (γ) solid solution matrix and MC carbide (M being mostly Ti and Mo). This also has been previously reported by other researchers.[1] SEM-EDS semiquantitative analysis of the MC carbide in the as-received alloy is shown in Table III. The carbide particles present in the alloy varied in size, ranging from about 2 μm to about 15 μm, and were randomly dispersed as intergranular and intragranular particles within the gamma matrix. MC-type carbides usually form in nickel-base superalloys during ingot solidification,[3] and the particles were reported to be metastable in nature with a tendency toward dissolution or dissociation during high-temperature thermal treatment.[3,4]

Figure 2 shows a SEM micrograph of the HAYNES alloy 282 alloy subjected to the recommended standard heat treatment (STHT) for the alloy at 1423 K (1150 °C) for 2 hours + water quenching followed by aging at 1283 K (1010 °C) for 2 hours + air-cooled + 1061 K (788 °C) for 8 hours + air-cooled, which resulted in coarsening of the grains to produce an average grain size of ≈300 μm. The STHT microstructure consists of intergranular and intragranular primary MC-type carbides. Fine submicron size precipitates were formed along the grain boundaries and at the phase boundary between the MC carbides and the γ matrix. The principal strengthening phase of the alloy, γ' precipitates, however, was not observed by the SEM. The nature of the fine precipitates at the MC/γ interface and along the grain boundaries could not be identified by using the SEM, because of the inherent limitation of the spatial resolution of the SEM-EDS to reliably analyze submicron particles. Therefore, TEM was used to further analyze the microconstituents in the alloy.

Figure 3(a) shows a TEM high-angle annular dark-field (HAADF) image of the STHT sample, and Figure 3(b) presents the results of TEM-EDS line scans across the matrix and intergranular particles shown in Figure 3(a). The EDS line scan results indicate that there are three types of particles along the grain boundary: Cr rich, Mo rich, and Ti rich (Figure 3(b) and Table IV). A typical TEM-EDS spectrum from Mo-rich particles (Figure 4) shows a boron peak, suggesting that the Mo-rich particles could be borides. Selected area electron diffraction was used to determine the crystallographic structure of the Cr-rich, Mo-rich, and Ti-rich particles. Analysis of the selected area diffraction patterns (SADPs) obtained from different zone axes of the Cr-based phase (Figures 5) showed that the particles are fcc $M_{23}C_6$ carbides with lattice parameter a = 1.06 nm. This type of carbides was reported in nickel-base

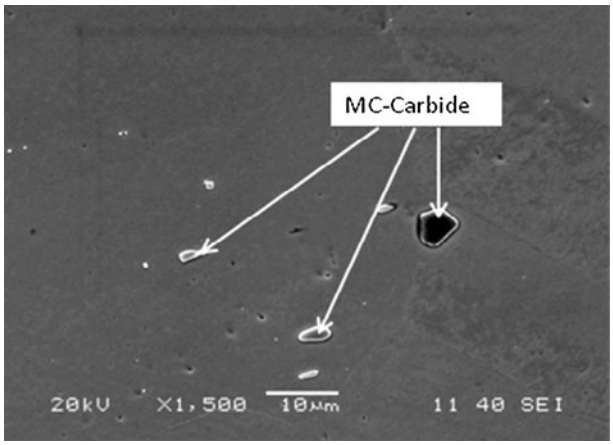

Fig. 1—SEM micrograph of as-received HAYNES alloy 282 showing MC-carbide particles.

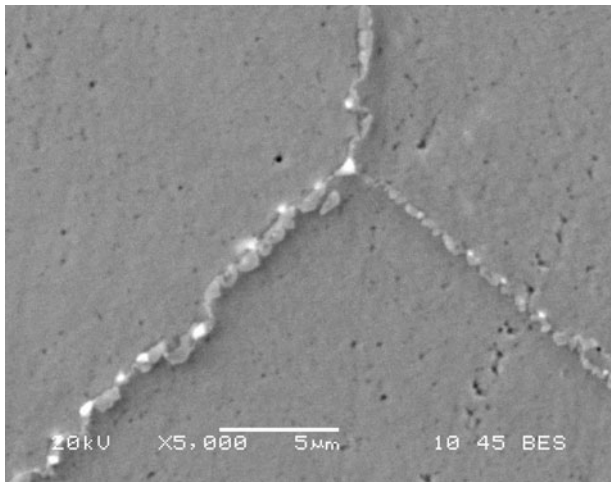

Fig. 2—SEM micrograph of HAYNES alloy 282 in standard heat treatment condition showing submicron intergranular precipitates.

Table III. EDS Semiquantitative Chemical Composition Analysis (Weight Percent) of Metallic Elements in Phases Present in the As-Received and Standard Heat-Treated HAYNES Alloy 282

		Elements							
Secondary Phases	Ti	Mo	Cr	Al	Co	Mn	Si	Fe	Ni
MC carbide*	66.13	29.25	2.31	—	0.29	—	0.05	0.04	1.93
MC carbide	60	34.87	2.95	—	0.43	0.03	0.51	0.46	0.60
Cr-rich phase	—	15.01	76.26	0.11	2.49	0.19	0.29	0.52€	5.14
Mo-rich phase	2.86	42.95	22.65	1.22	7.44	—	1.64	0.41	20.83

*As-received.

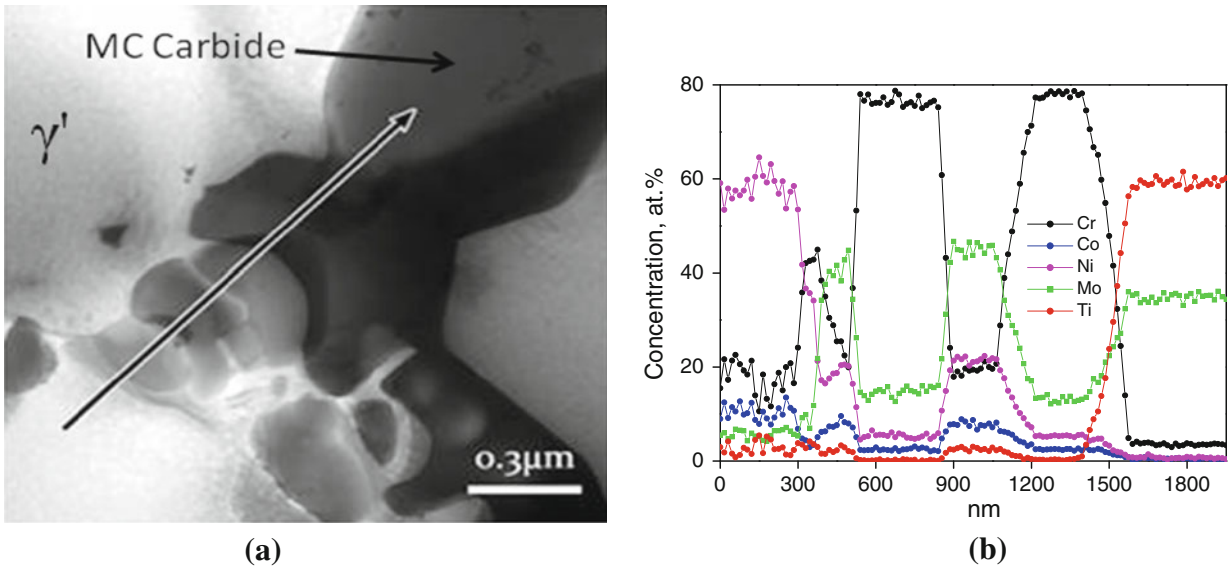

Fig. 3—(*a*) STEM-HAADF image of the intergranular precipitates in standard heat-treated HAYNES alloy 282. (*b*) Results of TEM-EDS line scans of the intergranular precipitates in (a).

Table IV. DSC Phase Transformation Temperatures in HAYNES Alloy 282

Reaction	Transformation Temperature ±5 °C
Liquidus	1633 K (1360 °C)
Solidus	1517 K (1244 °C)
γ' solvus	1273 K (1000 °C)

superalloys, and the carbides are known to form by precipitation reaction from carbon-supersaturated γ matrix during the aging heat treatment [1023 K to 1328 K (750 °C to 1055 °C)] that normally follows solution treatment;[3–7] *i.e.*,

$$\gamma \Leftrightarrow M_{23}C_6 + \gamma \qquad [1]$$

It has been also reported that they could likewise form by phase reaction between MC-type carbide and γ matrix[3] *via* the following type of phase transformation reaction:

$$\gamma + MC \Leftrightarrow M_{23}C_6 + \gamma' \qquad [2]$$

The $M_{23}C_6$ particles formed by this second reaction are located in the vicinity of degenerated MC particles. Figure 6 shows SADPs obtained from different zone axes of the Mo-B rich particles. The analysis of the diffraction patterns showed that the particles are tetragonal (bct) M_5B_3 boride particles with lattice parameters $a = 0.56$ nm, $c = 1.01$ nm, and $c/a = 1.83$. To the authors' knowledge, this type of phase, M_5B_3 boride, was not previously reported in the HAYNES alloy 282. It was proposed that the addition of boron to nickel-base superalloys can influence the structure and chemistry of grain boundary precipitates.[8,9] The solid solubility of boron in austenitic (γ) alloys is very low. For example, Goldschmidt[10] reported a maximum solubility of 97 ppm of boron at 1398 K (1125 °C) in 18 pct Cr-15 pct Ni stainless steel. The solubility decreases rapidly with decreasing temperature and becomes less than 30 ppm at 1173 K (900 °C). Furthermore, the size of boron atoms is larger than the common interstitial elements in nickel (*e.g.*, C) and smaller than substitutional elements such as Co and Cr. The size misfit of boron atoms in both the substitutional and interstitial sites in austenitic lattice implies that it would be energetically favorable for boron atoms to segregate to loosely packed regions such as grain boundaries and other incoherent phase boundaries. Interfacial segregation of boron was experimentally observed in a number of superalloys and austenitic alloys.[11–13] A grain boundary characterization study of boron segregation in an austenitic alloy by secondary ion mass spectroscopy, however, indicated that, during heat treatment, boron tends to have stronger affinity for partitioning into second-phase particles rather than remaining in solid solution form on grain boundaries.[9,11–15] This may explain the formation of the M_5B_3 boride particles observed in the standard heat-treated HAYNES alloy 282. Furthermore, the analysis of diffraction patterns obtained from the Ti-rich particles confirmed the particles to be fcc MC with lattice parameter $a = 0.428$ nm (Figure 7). The γ' precipitates, which could not be observed by the SEM, were revealed by the TEM (HAADF image in Figure 3(a) and the dark-field image in Figure 8(a)). The SADP taken from the [112] zone axis of the γ matrix (Figure 8(b)) shows strong superlattice reflections of γ' phase.

B. *Microstructure of Laser-Beam-Welded Haynes Alloy 282*

An optical micrograph of a general laser weld region in HAYNES alloy 282 subjected to the STHT, showing the fusion zone (FZ) and HAZ, is presented in Figure 9. Cracks were not observed in the FZ, and this is typical of all the welded specimens examined in this study,

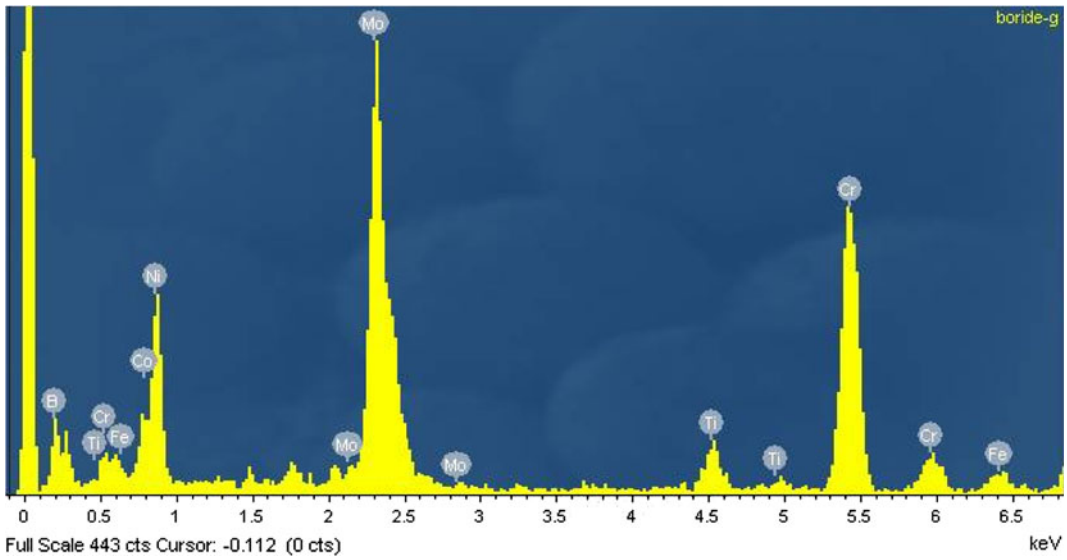

Fig. 4—TEM-EDS spectrum of the Mo-rich phase, which also shows boron peak.

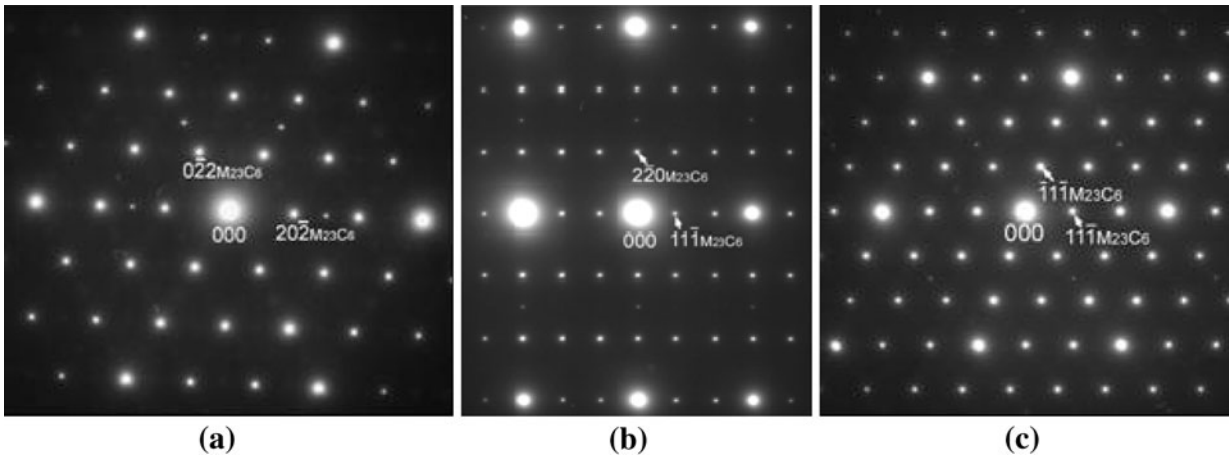

Fig. 5—SADP from (*a*) [111], (*b*) [112], and (*c*) [011] zone axes of the $M_{23}C_6$ carbide.

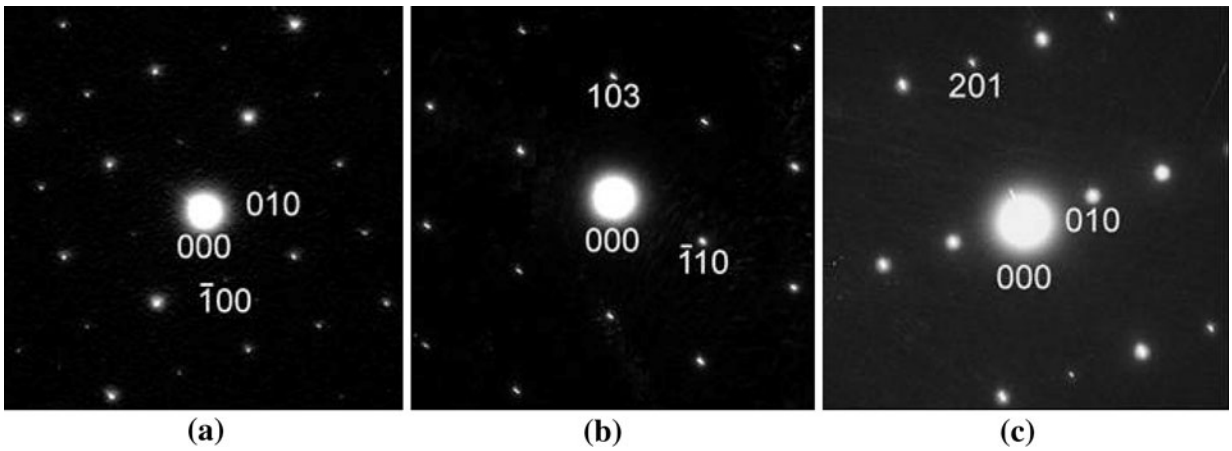

Fig. 6—SADP from (*a*) [001], (*b*) $[\bar{3}\bar{3}1]$, and (*c*) $[\bar{1}02]$ zone axes of the M_5B_3 boride.

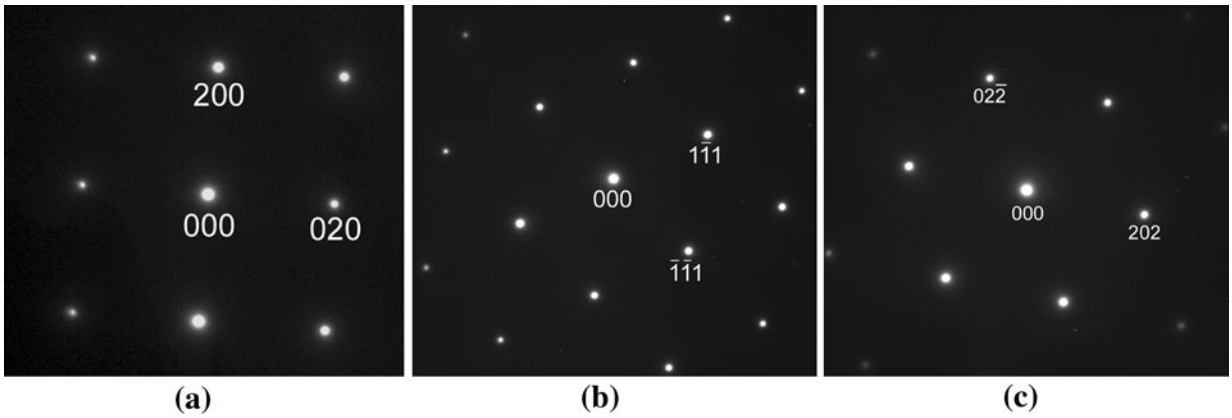

Fig. 7—SADP from (*a*) [001], (*b*) [011], and (*c*) [11] zone axes of the MC carbide.

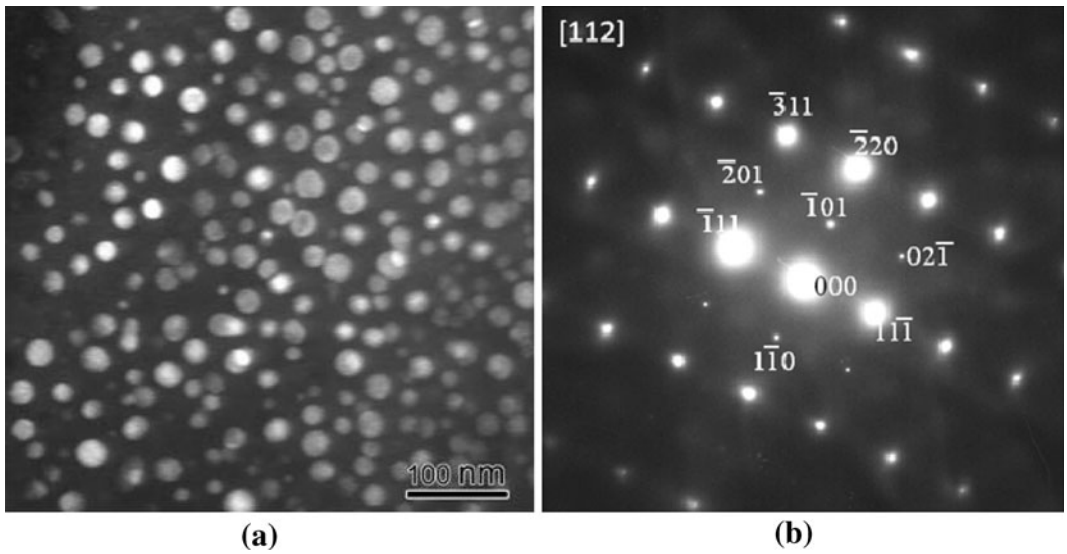

Fig. 8—(*a*) Dark-field image of γ' particles obtained using $(\bar{1}01)$ superlattice reflection. (*b*) [112] SADP showing the presence of superlattice reflections typical of $L1_2$ ordered lattice of γ' phase.

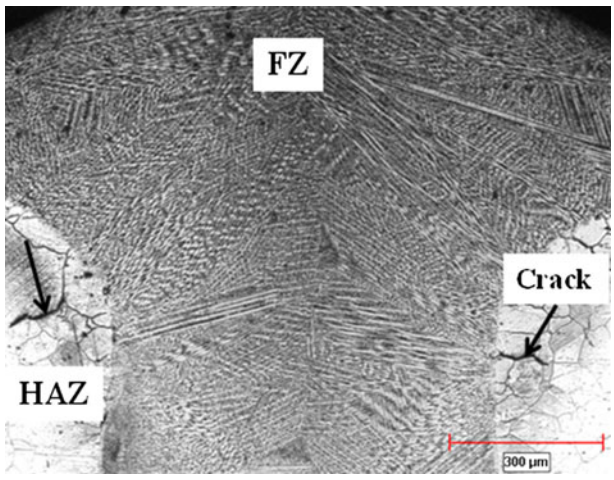

Fig. 9—Low magnification optical micrograph of weld FZ and HAZ regions showing cracks in the HAZ region.

irrespective of the preweld heat treatment. Although no FZ cracking was observed, the HAZ suffered a varying degree of intergranular cracking (Figure 10). Most of the cracks were located in the neck region of the keyhole shaped weld, in HAZ regions that are slightly away from the FZ. The cracks have irregular zigzag morphology, which is typical of intergranular liquation cracking.[16,17] HAZ grain boundary liquation cracking, caused by the formation of liquid phase along the intergranular region and subsequent decohesion along one of the intergranular solid-liquid interfaces under the influence of tensile stress generated during weld cooling, is known to occur in nickel-base superalloys.[16–18]

C. *Cause of Intergranular Haz Liquation Cracking in Haynes Alloy 282*

HAZ grain boundary liquation is widely accepted to occur either by nonequilibrium subsolidus melting or equilibrium supersolidus melting.[19,20] Although

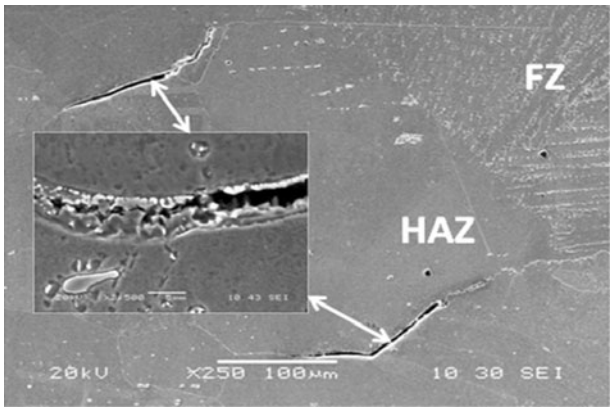

Fig. 10—SEM micrograph showing typical HAZ cracks.

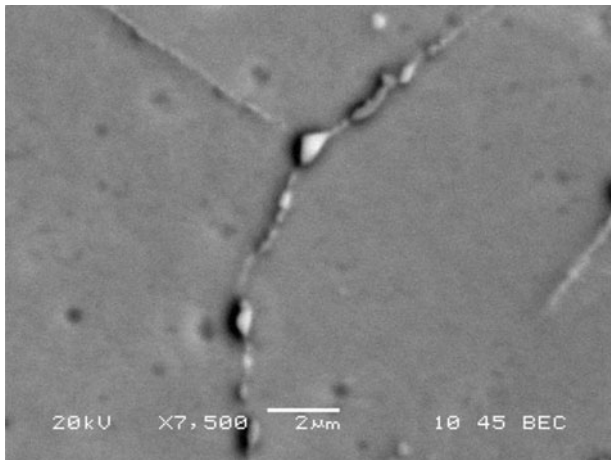

Fig. 11—SEM micrograph showing the persistence of grain boundary precipitates in a Gleeble simulation specimen that was rapidly heated to 1393 K (1120 °C).

supersolidus melting is expected to occur in all weldments due to heating above the equilibrium solidus temperature in certain regions, subsolidus grain boundary melting is more insidious and detrimental, as it extends both the effective melting temperature range and the size of the crack susceptible region in the HAZ.[18,21] In addition, subsolidus melting is also known to influence the nature of melting at supersolidus temperatures by pre-establishing local heterogeneities that are capable of altering the kinetics of reaction during subsequent heating.[22] One of the mechanisms used to explain the subsolidus formation of liquid film along grain boundaries is constitutional liquation of second-phase particles present in preweld material due to nonequilibrium reaction between the particles and the surrounding matrix.[16,23,24] The short integrated time and steep temperature gradient during welding thermal cycle induces microstructural variation over a relatively short distance in the HAZ of weldments. This makes detailed microstructural analysis and the relation between phase transition and peak temperature difficult to ascertain. The grain boundary liquation features observed in the present work suggest that the HAZ liquation involved significant subsolidus liquation. To enable a reliable verification of subsolidus liquation occurrence in the HAYNES alloy 282 during welding, the Gleeble thermomechanical simulation system was used to physically simulate its HAZ microstructure. A DSC study, using a NETZ-404C differential scanning calorimeter, was first performed to determine the main equilibrium phase transformation temperatures in the new alloy, and the results are listed in Table IV. HAYNES alloy 282 specimens were rapidly heated by the Gleeble system to peak temperatures below the equilibrium solidus temperature of the alloy, from 1323 K to 1473 K (1050 °C to 1200 °C), to evaluate the response of the alloy to the rapid welding thermal cycle.

Microstructural examination of the Gleeble specimens simulated at the peak temperatures up to 1393 K (1120 °C) showed that the second-phase precipitates along the grain boundaries in the alloy remained largely unaffected by the Gleeble simulation thermal cycle (Figures 11(a) and (b)). However, in specimens rapidly heated to 1423 K and 1443 K (1150 °C and 1170 °C) and held for 1 second, complete dissolution of the intergranular particles occurred and widening of grain boundary regions was observed (Figure 12(a)). An increase of the holding time at the peak temperatures to 3 seconds resulted in reduction in the occurrence of the widened grain boundaries (Figure 12(b)). This behavior is consistent with the grain boundary liquation caused by constitutional liquation of second-phase particles.[16] A major consequence of intergranular liquation in nickel-base superalloys is poor hot ductility under tensile loading. In order to further confirm the occurrence of liquation on the widened grain boundaries observed at 1423 K and 1443 K (1150 °C and 1170 °C), the hot ductility of the alloy was evaluated by subjecting Gleeble specimens to tensile loading, first, after holding for 0.1 seconds at various peak temperatures, and the results are presented in Figure 13. The alloy initially exhibited high hot ductility, but the ductility dropped to a significantly low level at 1423 K (1150 °C) and approached zero around 1443 K (1170 °C). As earlier stated, widened grain boundaries were observed at the peak temperatures 1423 K and 1443 K (1150 °C and 1170 °C), at which the alloy exhibited considerably poor ductility. On increasing the holding time from 0.1 to 3 seconds during the hot ductility test at 1443 K (1170 °C), improvement in ductility from 3 to 26 pct was notably observed. The increase in ductility with holding time correlates with the observed reduction in thickness of widened grain boundaries with increase in holding time, which can be attributed to resolidification of intergranular metastable liquid, since the liquid phase reduces hot ductility.[16]

Previous studies showed that another verifiable way of confirming grain boundary liquation is by fractography study of crack surface.[25–27] SEM study of fractured surface of Gleeble hot ductility specimens confirmed brittle intergranular failure in specimens tested at 1423 K and 1443 K (1150 °C and 1170 °C) with 0.1 seconds holding time, which correlates with the loss of ductility observed at these temperatures (Figure 14(a)). Higher magnification examination of

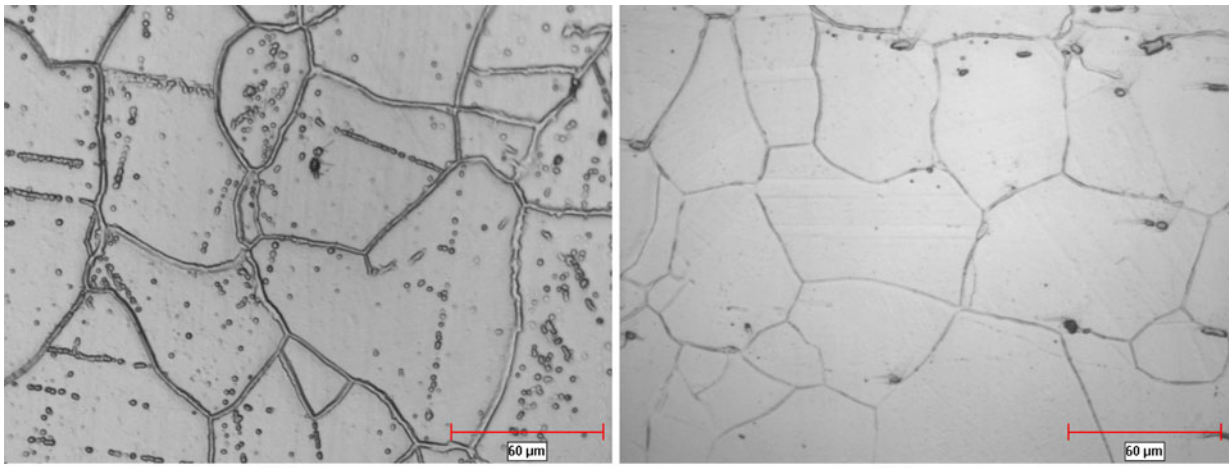

Fig. 12—(*a*) Optical micrograph showing widened grain boundaries in a Gleeble simulation specimen rapidly heated to 1443 K (1170 °C), held for 1 s, and water quenched. (*b*) Optical micrograph showing reduction in the occurrence of widened liquated grain boundaries in a Gleeble simulation specimen rapidly heated to 1443 K (1170 °C), held for 3 s, and water quenched.

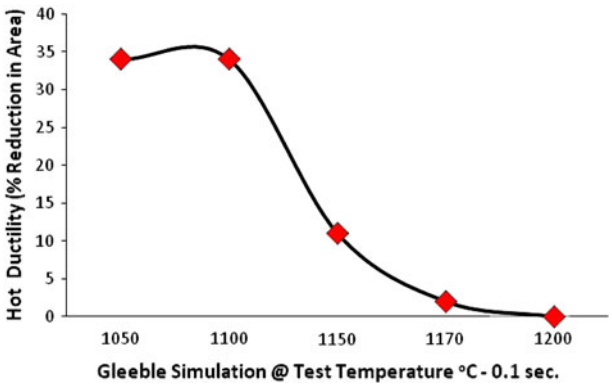

Fig. 13—Variation of hot ductility of HAYNES alloy 282 with peak temperature after a holding time of 0.1 s.

the grain surfaces revealed regular roundish surface features all over the grain facets (inset in Figure 14(a)), which were reported to be an indication of resolidified intergranular liquid phase.[25] For the sake of clarity and comparison, Figure 14(b) shows the fractured surface of a hot ductility test specimen tested at 1393 K (1120 °C), where the alloy exhibits high ductility. The specimen exhibited a ductile transgranular failure mode in contrast to the brittle intergranular fracture observed in the 1423 K and 1443 K (1150 °C and 1170 °C) specimens. Therefore, degradation of capability of alloy 282 to accommodate welding stresses, due to the embrittling effect of intergranular liquation caused by liquation of second-phase precipitates is an important factor contributing to the susceptibility of the material to HAZ cracking during the laser welding. A careful analysis of the Gleeble-simulated specimens did not show any evidence of constitutional liquation of MC carbides at the peak temperatures 1423 K and 1443 K (1150 °C and 1170 °C), which is consistent with the reported liquation behavior of the carbides in nickel-base superalloys.[28] Also, Owzarski[29] in their study of weldability of nickel-base superalloys indicated that $M_{23}C_6$ particles would undergo solid-state reaction well below the solidus temperature and would not constitutionally liquate during welding. It is, thus, possible that the subsolidus intergranular liquation observed at 1423 K and 1443 K (1150 °C and 1170 °C) is mainly caused by constitutional liquation reaction of the M_5B_3 borides identified for the first time in this work. In order to verify this possibility, HAYNES alloy 282 specimens subjected to heat treatment at 1373 K (1100 °C), which dissolves the $M_{23}C_6$ carbides and leaves the M_5B_3 borides as the main intergranular precipitates (Figure 15(a)), were rapidly heated by Gleeble system to various peak temperatures. The Gleeble simulation results showed that the grain boundary liquation still occurred at 1423 K and 1443 K (1150 °C and 1170 °C), despite the exclusion of the $M_{23}C_6$ carbides, indicating that the subsolidus nonequilibrium liquation reaction is attributable to constitutional liquation of the M_5B_3 borides (Figure 15(b)). Figure 15(c) shows results of the SEM-EDS line scan across a M_5B_3 particle along a liquated grain boundary region in 1373 K (1100 °C) heat-treated Gleeble-simulated specimen. The enrichment of the boride with Mo and the depletion of Cr in the boride, shown by the line scan results, are consistent with results of TEM-EDS analysis of the boride phase (Figure 3).

D. *Factors Aiding Haz Liquation Cracking in the Haynes Alloy 282*

In many of the available studies on intergranular liquation cracking, it is reported that the mere occurrence of liquation is judged to be inadequate to induce a microstructure susceptible to cracking. The liquid phase must of necessity wet, infiltrate, and spread along the grain boundary region in a continuous or semicontinuous fashion, replacing the solid-solid interfacial energy

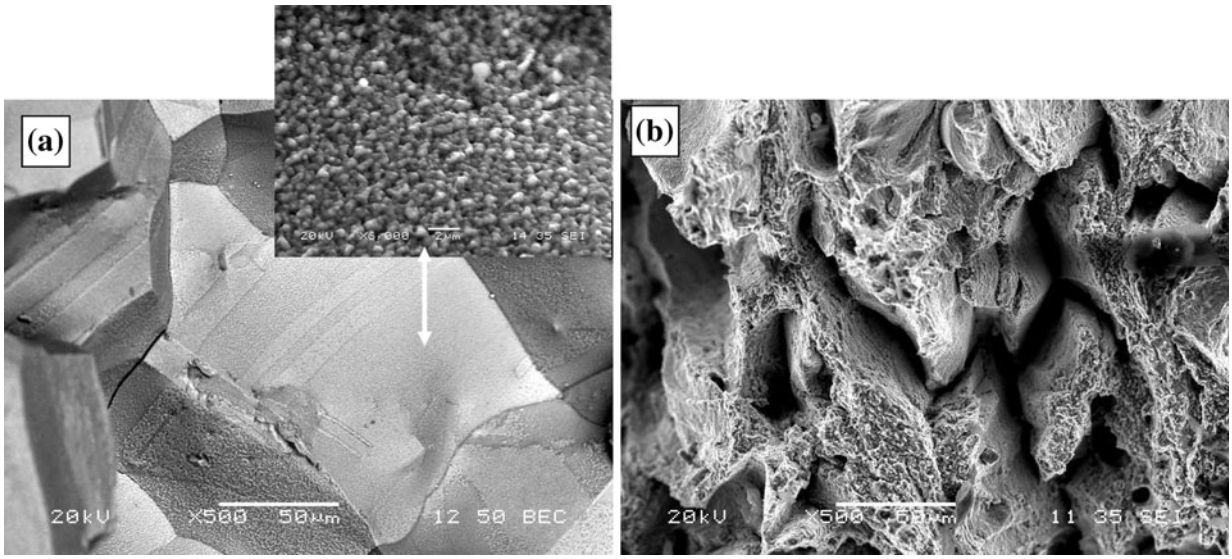

Fig. 14—SEM fractograph of Gleeble specimens tested at (*a*) 1443 K (1170 °C) after holding for 0.1 s (inset shows resolidified liquid phase). (*b*) 1393 K (1120 °C) after holding for 0.1 s.

along the grain boundary with a weaker solid-liquid interfacial energy.[30] Ineffective wetting of grain boundary regions by the liquid film will result in the liquid existing in isolated pockets that allow for substantial solid-solid intergranular contact. To a first approximation, the distribution of intergranular liquid can be treated in accordance with the relationship proposed by Smith:[31]

$$\gamma_{gb} = 2\gamma_{SL}\mathrm{Cos}\theta \qquad [3]$$

where θ is the wetting angle, γ_{gb} is the grain boundary energy, and γ_{SL} is the solid-liquid interface energy.

From Eq. [3], it can be seen that for a given grain boundary energy, the lower the solid-liquid interface energy, the lower will be the wetting angle and the easier it will be for such a liquid to wet and spread along the grain boundary. The presence of boron atoms in the intergranular liquid produced by liquation of the M_5B_3 borides could substantially aid the wetting behavior of the liquid through the influence of the surface-active boron atoms in lowering the solid-liquid interface energy along grain boundary. In an alternate or complementary case, as apparent from Eq. [3], for a given solid-liquid interfacial energy, the higher the grain boundary energy, the higher is the tendency for it to be wetted and penetrated by liquid phase. In the present study, EBSD analysis of grain boundary character showed that most of the grain boundaries in the as-received and heat-treated HAYNES alloy 282 are more of a "random" nature with higher order of "Σ" values (Figure 16). Random high-angle grain boundaries are inherently of higher energy than special boundaries. The fact that most of the grain boundaries in the HAYNES alloy 282 are of the high energy type could be another factor that enables intergranular wetting and penetration by liquid film in the alloy. Guo *et al.*[12] and Kokawa *et al.*[32] confirmed that liquid penetration at grain boundary was greatest at high-angle boundaries and was relatively insignificant at low-angle boundaries. Furthermore, the metastable liquid produced by the constitutional liquation of intergranular second-phase particles always reacts with the adjacent solid grain through back-diffusion of solute atoms across the solid-liquid interface. In these situations, the nonequilibrium solid-liquid interfacial energy is extremely low,[33] which would make the liquid effectively wet the grain boundary and exhibit extensive penetration. A theoretical model developed for describing the penetration of liquid phase along a grain boundary showed that the grain boundary penetration requires an undersaturated solid.[34] This is essentially the situation prevalent in the subsolidus HAZ regions during nonequilibrium rapid heating and cooling of the welding operation. During the rapid heating cycle, decomposition of intergranular M_5B_3 borides can result in the release of boron atoms along grain boundary regions. Aside from aiding grain boundary wetting, the boron released from the M_5B_3 borides is a potent melting point depressing element in nickel alloys. The enrichment of intergranular regions with boron atoms can reduce the starting temperature for grain boundary liquation during heating and also reduce the terminal solidification temperature during cooling. Previous studies[35,36] showed that on-cooling hot ductility behavior is dependent on the hot ductility behavior during heating. On-heating ductility behavior can thus provide an indication of expected ductility behavior during cooling. Any factor that reduces the on-heating ductility will reduce the ductility during cooling. As an example, any factor that decreases on-heating zero ductility temperature will reduce the ductility recovery temperature during cooling. Ductility recovery temperature during cooling is generally lower than the zero ductility temperature during heating.[35,36] Therefore, in the present work, the grain boundary

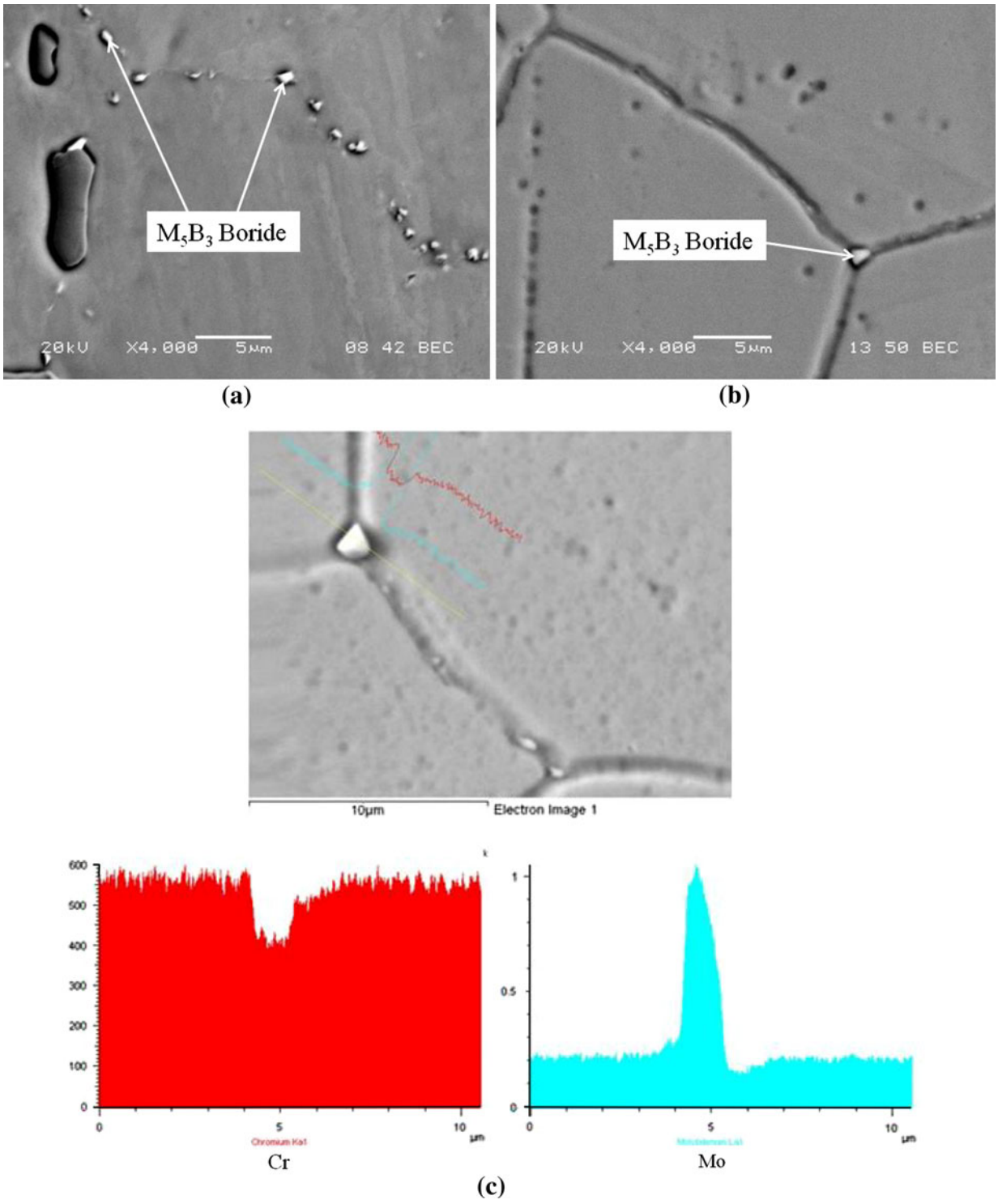

Fig. 15—SEM micrographs of (*a*) solution-heat-treated specimen at 1373 K (1100 °C) before Gleeble simulation. (*b*) Gleeble simulation specimen rapidly heated to 1443 K (1170 °C) and held for 1 s, which shows intergranular M_5B_3 particle associated with liquated and widened grain boundaries. (*c*) Results of SEM-EDS line scans across a M_5B_3 particle along the liquated grain boundary region.

liquation, which reduced the on-heating zero ductility temperature, would in effect enlarge the brittle temperature range and delay ductility recovery of the HAZ during cooling, both of which would promote susceptibility to liquation cracking. Therefore, the reaction of the intergranular M_5B_3 boride particles with the surrounding fcc solid solution matrix to produce liquation at subsolidus temperatures constitutes a major factor that reduces the resistance of the newly developed alloy to weld HAZ cracking.

E. *Preweld Heat Treatment to Improve Resistance of the Haynes Alloy 282 to Haz Cracking*

Since the liquation of the M_5B_3 borides is found as the major factor causing HAZ cracking in the HAYNES alloy 282, heat treatments of the alloy at 1323 K to 1423 K (1050 °C to 1150 °C) for 2 hours were performed to study the dissolution of the boride particles. The results showed that no major dissolution of the boride particles occurred at 1323 K (1050 °C), but an increase in heat treatment temperature to 1353 K to 1373 K (1080 °C to 1100 °C) (Figure 15(a)) resulted in significant dissolution of the particles, such that very few isolated particles remain after heat treatment at these temperatures. A further increase in temperature to 1393 K (1120 °C) and above resulted in complete dissolution of the boride particles (Figures 17(a) and (b)). Specimens subjected to heat treatment at 1323 K to 1423 K (1050 °C to 1150 °C) and air-cooled were laser welded to examine the effect of the boride dissolution on susceptibility to HAZ cracking. Three different welding test coupons were used for each preweld heat treatment condition. Ten weld cross sections were prepared from each test coupon for the crack measurement. The average values of the total crack length (TCL) in the 10 weld cross sections from the 3 different welded test coupons for each of the preweld heat treatment conditions are presented in Figure 18. As shown by the results, the presence of the boride particles in the 1323 K (1050 °C) heat-treated specimen resulted in significant HAZ cracking. Reduction in the volume fraction of the borides by heat treatment at 1353 K to 1373 K (1080 °C to 1100 °C) appreciably reduced the level of cracking. Interestingly, however, complete dissolution of the boride particles by preweld heat treatment at 1393 K (1120 °C) and above exacerbates rather than reduces the cracking. The reason why complete dissolution of the borides, which are known to aid susceptibility to cracking by constitutionally liquating during welding, caused an increase rather than decrease in cracking was investigated.

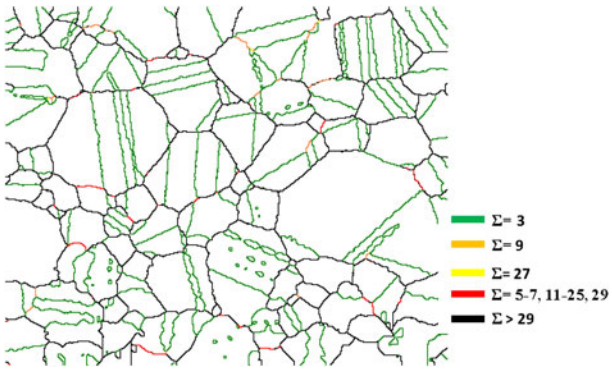

Fig. 16—EBSD analysis of grain boundary character distribution in the HAYNES alloy 282. High-angle grain boundaries $\Sigma > 29$ are shown in black.

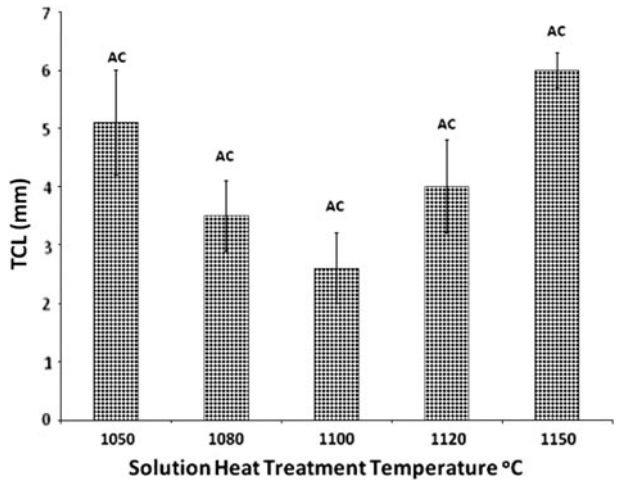

Fig. 18—Variation of total crack length in HAYNES alloy 282 subjected to preweld solution heat treatment at different temperatures followed by air cooling.

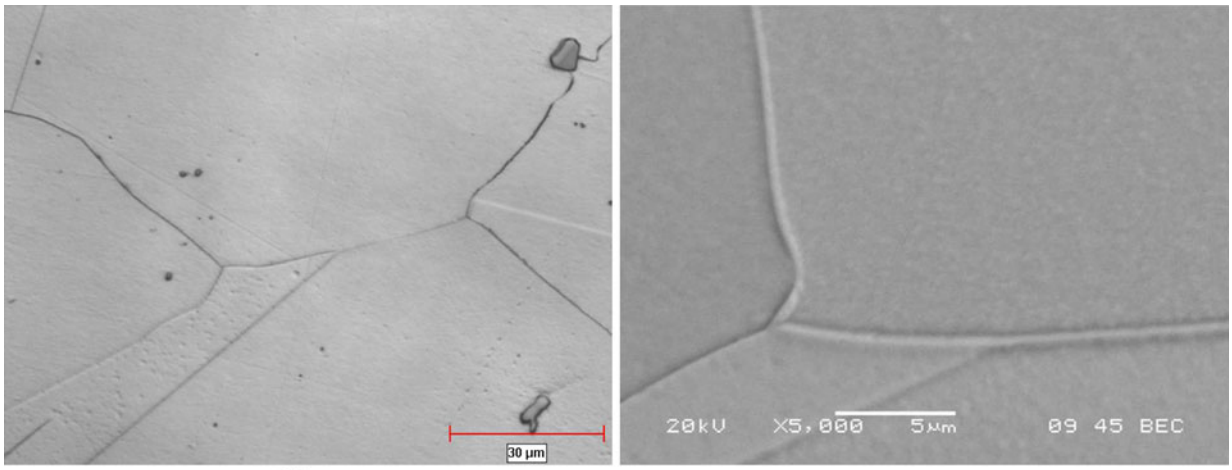

Fig. 17—(*a*) Optical and (*b*) SEM micrographs of a specimen solution heat treated at 1423 K (1150 °C) showing the grain boundaries free of M_5B_3 boride particles.

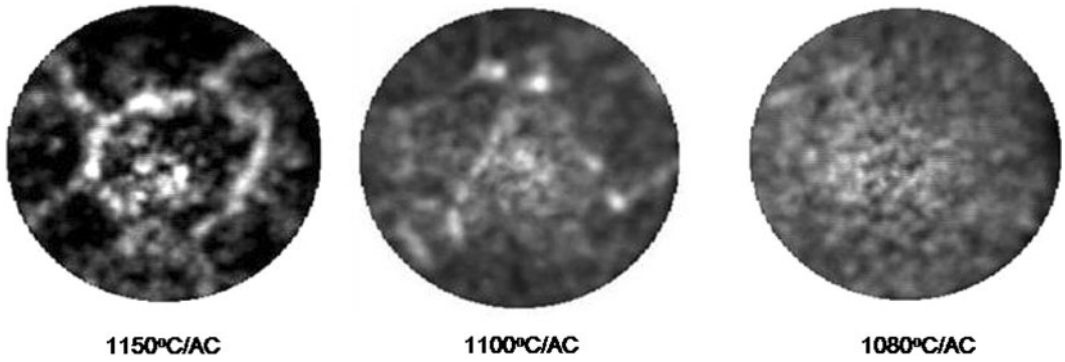

Fig. 19—SIMS image showing an increase in nonequilibrium segregation of boron with an increase in heat treatment temperature (air-cooling condition).

At 1393 K (1120 °C) and above, which are above the solvus temperature of the boride phase, all the boron atoms initially tied down in the boride particles are released into the surrounding austenitic, γ, matrix phase. As earlier stated, the size misfit of boron atoms for both the substitutional and interstitial sites in austenitic lattice makes it energetically favorable for boron atoms to segregate to loosely packed regions such as grain boundaries. When alloys are quenched from high temperature, the equilibrium vacancy concentration falls and vacancies migrate to interfaces such as grain boundaries, where they can be readily annihilated. Solute atoms in a crystal, especially surface-active elements such as boron, have an associated strain energy that can be relieved by pairing with vacancy to form a vacancy-solute complex. Vacancy flow, with an associated solute flux, to annihilation sites such as grain boundaries can, thus, occur during cooling from high temperature, which is a phenomenon generally referred to as nonequilibrium elemental intergranular segregation.[37,38] Therefore, nonequilibrium segregation of boron atoms, released by the dissolution of boride particles, to grain boundary regions can occur during the preweld heat treatments at 1393 K (1120 °C) and above, the extent of which is expected to increase with temperature. Secondary ion mass spectroscopy analysis of the alloy confirmed nonequilibrium intergranular segregation of boron in the alloy. An increase in heat treatment temperature resulted in increased nonequilibrium intergranular boron segregation during cooling (Figure 19). Nonequilibrium intergranular segregated boron atoms can damage cracking resistance by causing grain boundary liquation in the HAZ during welding, similar to what is caused by constitutional liquation of the M_5B_3 boride particles. This may explain the observed increase in HAZ cracking with an increase in preweld heat treatment temperature above 1393 K (1120 °C). Moreover, nonequilibrium segregation is very sensitive to cooling rate from heat treatment temperature. Rapid cooling rate, such as the one involved during water quenching, can cause excess solute-vacancy complex to be "frozen in," and reduce nonequilibrium segregation, since sufficient time would not be available for the migration of the solute-vacancy complex to annihilation sites. At intermediate cooling rates, such as in air cooling, vacancy-solute complexes can have sufficient time to migrate to annihilation sites, which may result in a more severe grain boundary elemental segregation. A much slower cooling rate such as furnace cooling, however, can cause desegregation of solute atoms, which would eventually result in a less severe intergranular segregation.[37] Hence, a more severe grain boundary segregation of boron and concomitant higher level of HAZ cracking is expected in air-cooled than in water-quenched and furnace-cooled heat-treated specimens. This was investigated in the present work by examining the extent of HAZ cracking in ten weld cross sections from each of three different welded test coupons subjected to preweld heat treatment at 1423 K (1150 °C) and water-quenched, air-cooled, and furnace-cooled. As shown by the results presented in Figure 20, the highest level of cracking occurred in the air-cooled condition. Notwithstanding the significantly higher hardness of the furnace-cooled specimen compared to the air-cooled specimen (Figure 21), which normally could be expected to aid cracking, cracking is rather greater in the air-cooled condition, where more nonequilibrium boron segregation is expected. The results, thus, indicate that aside from constitutional liquation of the M_5B_3 borides, nonequilibrium segrega-

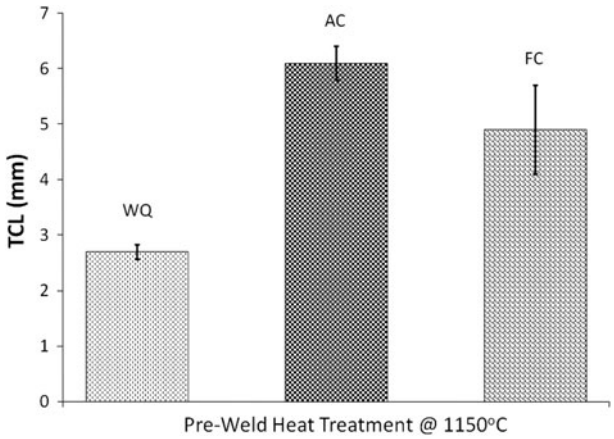

Fig. 20—Total crack length in HAYNES alloy 282 heat treated at 1423 K (1150 °C) and water-quenched (WQ), air-cooled (AC), and furnace-cooled (FC).

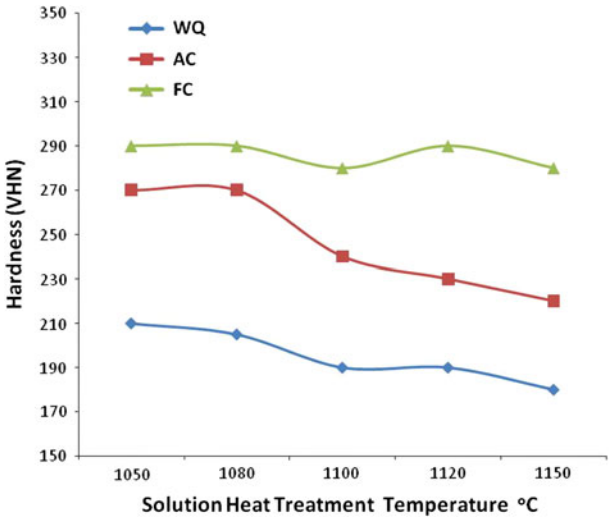

Fig. 21—Variation of HAYNES alloy 282 hardness with solution heat treatment temperature and for different cooling conditions.

tion of boron atoms, released by the dissolution of the boride particles during preweld heat treatment, is another attributable factor causing susceptibility to HAZ cracking in the new HAYNES alloy 282.

Accordingly, a viable approach to effectively reduce HAZ cracking in the alloy could be to reduce the volume fraction of the liquating M_5B_3 boride particles, as much as possible, by preweld heat treatment while minimizing nonequilibrium boron segregation. The results of the work performed in this research suggest that this is possible by using the preweld heat treatment at 1353 K to 1373 K (1080 °C to 1100 °C), as the results of the TCL from three different welded test coupons (Figures 18 and 20) consistently showed that the specimens subjected to preweld heat treatment at 1353 K to 1373 K (1080 °C to 1100 °C) produced the lowest level of HAZ cracking compared to other heat treatment conditions. Even though the preweld heat treatments at 1353 K to 1373 K (1080 °C to 1100 °C) reduce cracking, cracks still occur in these conditions.

F. *Further Reduction in Haz Cracking Through Grain Refinement*

A further attempt was made in this work to study how to entirely prevent or minimize HAZ cracking in the 1353 K to 1373 K (1080 °C to 1100 °C) preweld heat treatment condition. As stated earlier, grain boundary liquation is found to be the primary material cause of susceptibility of the alloy to HAZ cracking. Miller and Chadwick[39] related the tensile stress, σ, required to cause cracking by overcoming the surface γ_{sl} tension at the solid-liquid interface on liquated grain boundaries to the liquid film thickness h by the equation

$$\sigma = 2\gamma_{sl}/h \qquad [4]$$

This implied that any factor that reduces the thickness of the intergranular liquid could, in effect, improve resistance to cracking by increasing the magnitude of

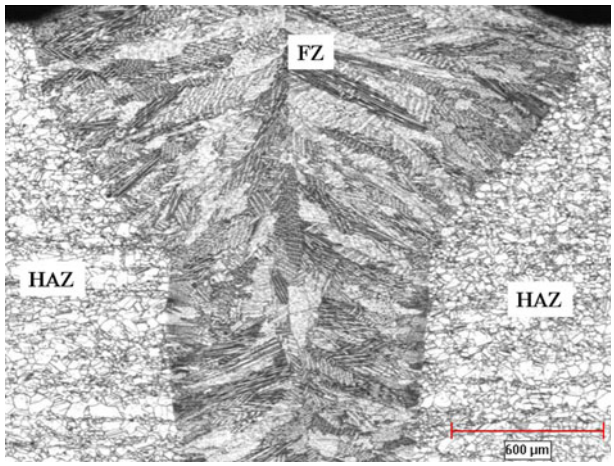

Fig. 22—Optical micrograph showing a typical crack-free weld section in HAYNES alloy 282 with the refined grains.

stress required to cause intergranular microfissuring. It is conceivable that the thickness of intergranular liquid, produced by the constitutional liquation of the few M_5B_3 borides present in the 1353 K to 1373 K (1080 °C to 1100 °C) condition, can be reduced by increasing the grain boundary surface area in the alloy to enable a wider spread of the intergranular liquid film. This idea was investigated by thermomechanically processing the alloy through cold working and annealing heat treatment to refine its grain size and increase the grain boundary surface area. The average grain size was reduced from about 140 μm to about 40 μm, and the material with refined grains was subjected to preweld heat treatment at 1353 K (1080 °C) for 2 hours, and laser beam welded. Interestingly, refining the grains to effectively reduce the thickness of intergranular liquid film produced by the liquation reaction of the few M_5B_3 borides in the 1353 K (1080 °C) condition produced crack-free welds in the alloy. A micrograph showing the crack-free weld region in the alloy with refined grains is presented in Figure 22. To the best knowledge of the authors, these are the first reported laser beam crack-free welds in the material. It was reported in the literature that weld cracking can be significantly influenced by material grain size;[40,41] however, very limited information is available on how grain size affects susceptibility to cracking. In the present work, it was found that formation of the crack-free welds is not attributable merely to reduced grain size without considering the effect of grain refinement on intergranular liquid produced by subsolidus liquation of the M_5B_3 borides. The Gleeble hot ductility test showed that enhanced resistance to cracking, through improved high-temperature ductility, did not occur with reduction in grain size when the material was free of the M_5B_3 borides (Figure 23). In contrast, however, when the liquating M_5B_3 borides were present in the material, reduction in grain size produced a significant increase in high-temperature ductility of the material (Figure 24). These, thus, indicate that a crucial role of grain size in enhancing material resistance to HAZ cracking is by improving hot ductility through its influence on

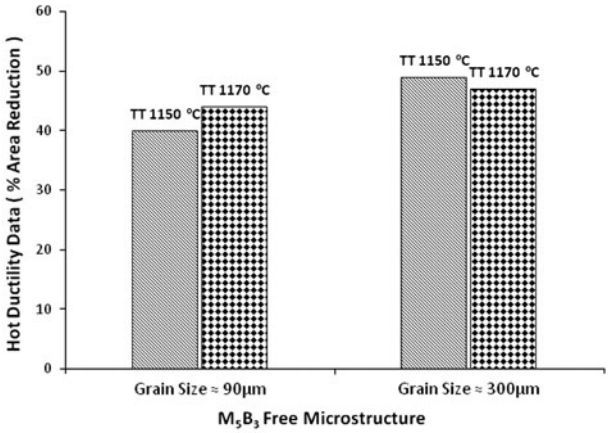

Fig. 23—Hot ductility of HAYNES alloy 282 without M_5B_3 borides and with different grain sizes at test temperatures (TTs) 1443 K and 1423 K (1150 °C and 1170 °C).

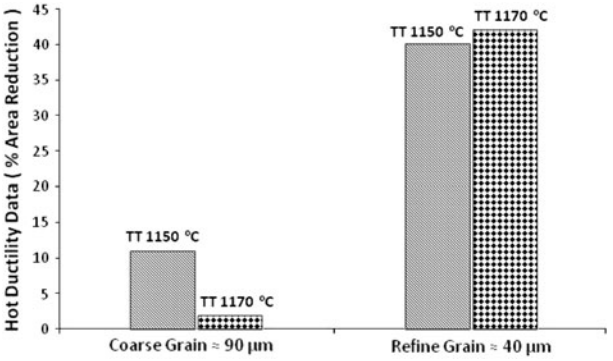

Fig. 24—Hot ductility of HAYNES alloy 282 containing M_5B_3 borides with different grain sizes at TTs 1443 K and 1423 K (1150 °C and 1170 °C).

intergranular liquation. The understanding enabled by this study and the resultant approach found effective to produce crack-free welds through grain refinement, coupled with an appropriate preweld heat treatment, may also be applicable to other difficult-to-weld nickel-base superalloys.

IV. SUMMARY AND CONCLUSIONS

The microstructures of heat-treated, laser-beam-welded, and Gleeble thermomechanically simulated specimens of the newly developed HAYNES alloy 282 were systematically studied to better understand the fundamental cause of HAZ cracking and how to prevent the cracking problem in the material. The results of the study produced the following salient information.

1) Analytical transmission electron microscopy revealed for the first time that in addition to $M_{23}C_6$ carbides, the grain boundaries in standard heat-treated Hayne alloy 282 contain submicron M_5B_3 boride particles, which were previously unidentified in the material.
2) A careful microstructural study of laser-welded specimens and Gleeble thermomechanical simulation revealed that a fundamental cause of HAZ cracking in the material is subsolidus liquation reaction of the newly identified M_5B_3 boride particles.
3) Complete dissolution of the liquating M_5B_3 borides by preweld heat treatment exacerbated, instead of lessening, susceptibility of the alloy to HAZ cracking, which is attributable to nonequilibrium intergranular segregation of boron atoms released by the dissolution of the boride particles.
4) The research shows that in order to minimize the HAZ cracking, a preweld heat treatment to reduce, as much as possible, the volume fraction of the M_5B_3 borides, while minimizing nonequilibrium grain boundary boron segregation, is required, which is found possible by heat treating the alloy at 1353 K to 1373 K (1080 °C to 1100 °C).
5) Further improvement in cracking resistance was produced by subjecting the material to thermomechanically induced grain refinement, which resulted in crack-free welds.
6) While grain size was previously reported to influence weld cracking in superalloys, Gleeble hot ductility testing in the present work showed that a crucial role of grain size in enhancing material resistance to HAZ cracking is by improving hot ductility through its influence on grain boundary liquation.

ACKNOWLEDGMENTS

The authors appreciate the financial support provided by NSERC, material supply by HAYNES International Inc., and laser welding by the Standard Aero Ltd. L.O. Osoba is grateful to the University of Manitoba for the award of University of Manitoba Graduate Fellowship.

REFERENCES

1. L.M. Pike: *Superalloy 2008*, TMS, Warrendale, PA, 2008, pp. 191–200.
2. L.O. Osoba and O.A. Ojo: *Mater. Sci. Technol.*, 2012, vol. 28 (4), pp. 431–36.
3. *Superalloys II*, C.T. Sims, N.S. Stoloff, and W.C. Hagel, eds., High Temperature Materials for Aerospace and Industrial Power, A Wiley-Interscience Publication, John Wiley and Sons Inc., New York, NY, 1987, pp. 97–133.
4. R.F. Decker and C.T. Sims:, in *The Superalloys*, T.C. Sims and W.C. Hagel, eds., John Wiley and Sons, New York, NY, 1972, pp. 33–77.
5. Y.L. Ge and J.Y. Wang: *Praktische Metallographie*, 1983, vol. 20 (11), pp. 554–61.
6. A.K. Koul and R. Castillo: *Metall. Trans. A*, 1988, vol. 19A, pp. 2049–66.
7. M.J. Donachie and S.J. Donachie: *Superalloy—A Technical Guide*, 2nd ed., ASM INTERNATIONAL, Materials Park, OH, 2002, pp. 211–86.
8. D.H. Maxwell, J.F. Baldwin, and J.F. Radavich: *Metall. Met. Form.*, 1975, pp. 332–38.
9. M. Kurban, U. Erb, and K.T. Aust: *Scripta Mater.*, 2006, vol. 54, pp. 1053–58.
10. H.J. Goldschmidt: *J. Iron Steel Inst.*, 1971, vol. 209, pp. 910–14.
11. X. Huang, M.C. Chaturvedi, N.L. Richards, and J. Jackman: *Acta Mater.*, 1997, vol. 45, pp. 3095–3107.
12. H. Guo, M.C. Chaturvedi, N.L. Richards, and G.S. McMahon: *Scripta Mater.*, 1999, vol. 40, pp. 383–88.

13. W. Chen, M.C. Chaturvedi, and N.L. Richards: *Metall. Trans. A*, 2001, vol. 32A, pp. 931–39.
14. O.A. Idowu, O.A. Ojo, and M.C. Chartuverdi: *Mater. Weld. J.*, 2009, vol. 88, pp. 179s–87s.
15. H.R. Zang, O.A. Ojo, and M.C. Chartuverdi: *Scripta Mater.*, 2008, vol. 58, pp. 167–70.
16. J.J. Pepe and W.F. Salvage: *Weld. J.*, 1967, vol. 46, pp. 411s–26s.
17. R.Vincent: *Acta Metall.*, 1985, vol. 33, pp. 1205–16.
18. W.A. Owezarki, D.S. Duvall, and C.P. Sullivan: *Weld. J.*, 1971, vol. 50, pp. 145–55.
19. B. Radhakrishnan and R.G. Thompson: *Metall. Trans. A*, 1991, vol. 22A, pp. 887–901.
20. O.A. Idowu, O.A. Ojo, and M.C. Chaturvedi: *Mater. Sci. Eng. A*, 2007, vol. 454, pp. 389–97.
21. W. Lin, J.C. Lippod, and W.A. Baeslack: *Weld. J.*, 1993, vol. 71 (4), pp. 135–53.
22. W.A. Owezarki, D.S. Duvall, and C.P. Sullivan: *Weld. J.*, 1966, vol. 44, pp. 145s–55s.
23. B. Jahnke: *Weld. J.*, 1982, vol. 61, pp. 343s–47s.
24. O.A. Ojo, N.L. Richards, and M.C. Chartuverdi: *Mater. Sci. Technol.*, 2004, vol. 20 (8), pp. 1027–34.
25. L.W. Wang: Ph.D. Thesis, The Ohio State University, Columbus, OH, 1991, pp. 120–80.
26. M. Qian: Ph.D. Thesis, The Ohio State University, Columbus, OH, 2001, pp. 54–130.
27. W.S. Scott: Ph.D. Thesis, The Ohio State University, Columbus, OH, 1991, pp. 226–65.
28. O.A. Ojo and M.C. Chartuverdi: *Metall. Mater. Trans. A*, 2007, vol. 38A, pp. 356–59.
29. W.A. Owzarski: *Proceedings of a Symposium Sponsored by the Weld Research Council*, New York, 1969, pp. 6–23.
30. J.C. Borland: *Br. Weld. J.*, 1960, vol. 7 (8), pp. 508–12.
31. C.S. Smith: *Trans. AIME*, 1948, vol. 175, pp. 15–51.
32. H. Kokawa, C.H. Lee, and T.H. North: *Metall. Trans. A*, 1998, vol. 29A, pp. 1627–34.
33. I.A. Askay, C.E. Hoge, and J.A. Pask: *J. Phys. Chem.*, 1974, vol. 78 (12), pp. 1178–83.
34. D. Chatain, E. Rabkin, J. Derenne, and J. Bernardin: *Acta Mater.*, 2001, vol. 49, pp. 1123–28.
35. W. Lin, J.C. Lippod, and W.A. Baeslack: *Weld. J.*, 1993, vol. 72, pp. 135s–53s.
36. C.D. Lundin, C.Y.P. Qiao, and R.W. Swindeman: *Proc. Int. Trends in Welding Science and Technology*, Gatlinburg, TN, 1993, pp. 801–06.
37. L. Karlson, H. Norden, and H. Odelius: *Acta Metall.*, 1988, vol. 36 (1), pp. 1–13.
38. L. Karlson and H. Norden: *Acta Metall.*, 1988, vol. 36 (1), pp. 35–48.
39. W.A. Miller and G.A. Chadwick: *Acta Metall*, 1967, vol. 15, pp. 607–14.
40. R.G. Thompson: *J. Met.*, 1988, vol. 7, pp. 44–48.
41. Nakkalil N.L. Richards and M.C. Charturvedi: *Acta Metall Mater.*, vol. 41 (12), pp. 3381–92.